

# Ages of Type Ia Supernovae Over Cosmic Time

Michael J. Childress<sup>1,2\*</sup>, Christian Wolf<sup>1,2</sup>, H. Jabran Zahid<sup>3,3</sup>

<sup>1</sup> *Research School of Astronomy and Astrophysics, Australian National University, Canberra, ACT 2611, Australia.*

<sup>2</sup> *ARC Centre of Excellence for All-sky Astrophysics (CAASTRO), Australian National University, Canberra, ACT 2611, Australia.*

<sup>3</sup> *Institute for Astronomy, University of Hawaii, 2680 Woodlawn Drive, Honolulu, HI 96822, USA.*

<sup>4</sup> *Smithsonian Astrophysical Observatory, Harvard-Smithsonian Center for Astrophysics, 60 Garden St., Cambridge, MA 02138, USA.*

11 September 2014

## ABSTRACT

We derive empirical models for galaxy mass assembly histories, and convolve these with theoretical delay time distribution (DTD) models for Type Ia supernovae (SNe Ia) to derive the distribution of progenitor ages for all SNe Ia occurring at a given epoch of cosmic time. In actively star-forming galaxies, the progression of the star formation rate is shallower than a  $t^{-1}$  SN Ia DTD, so mean SN Ia ages peak at the DTD peak in all star-forming galaxies at all epochs of cosmic history. In passive galaxies which have ceased star formation through some quenching process, the SN Ia age distribution peaks at the quenching epoch, which in passive galaxies evolves in redshift to track the past epoch of major star formation. Our models reproduce the SN Ia rate evolution in redshift, the relationship between SN Ia stretch and host mass, and the distribution of SN Ia host masses in a manner qualitatively consistent with observations. Our model naturally predicts that low-mass galaxies tend to be actively star-forming while massive galaxies are generally passive, consistent with observations of galaxy “downsizing”. Consequently, the mean ages of SNe Ia undergo a sharp transition from young ages at low host mass to old ages at high host mass, qualitatively similar to the transition of mean SN Ia Hubble residuals with host mass. The age discrepancy evolves with redshift in a manner currently not accounted for in SN Ia cosmology analyses. We thus suggest that SNe Ia selected only from actively star-forming galaxies will yield the most cosmologically uniform sample, due to the homogeneity of young SN Ia progenitor ages at all cosmological epochs.

**Key words:** supernovae: general, cosmology: dark energy

## 1 INTRODUCTION

Type Ia supernovae (SNe Ia) are believed to result from the thermonuclear disruption of a carbon-oxygen white dwarf (CO-WD) which reaches some instability condition through interaction with a binary companion (Hoyle & Fowler 1960). One possible scenario is the single-degenerate scenario (SD; Whelan & Iben 1973; Nomoto 1982), where a CO-WD accretes material from a non-degenerate main sequence (MS) star or red giant (RG) companion until reaching the critical Chandrasekhar mass. Alternatively, in the double-degenerate (DD) scenario, two CO-WDs coalesce after losing angular momentum to gravitational waves (Tutukov & Iungelson 1976; Tutukov & Yungelson 1979; Iben & Tutukov 1984; Webbink 1984). The binary evolution in these scenarios operates over a wide range of timescales from a few hundred Myr to a Hubble time. This manifests as a different instantaneous SN rate as a function

of progenitor age, referred to as the delay time distribution (DTD; for a review see Maoz & Mannucci 2012). Though it is never possible to pinpoint the exact progenitor age giving rise to a particular supernova, we will demonstrate how it is possible to derive the distribution of progenitor ages for a large sample of supernovae by combining the DTD with the star formation history of the parent stellar population of the SNe.

The existence of SNe Ia in passive host galaxies led to early speculation that SNe Ia could arise primarily from old stellar populations. However, SN Ia rates studies over the last decade suggest that the SN Ia rate in a galaxy is best parametrized by both the total stellar mass in the galaxy and its star formation rate (Mannucci et al. 2005; Scannapieco & Bildsten 2005; Sullivan et al. 2006; Mannucci et al. 2006; Aubourg et al. 2008; Li et al. 2011; Smith et al. 2012). This led to the “two-component” (or “A+B”) model description wherein SNe Ia can arise from both old (or “tardy”) and young (or “prompt”) progenitors. Further measurements of SN Ia rates show that the SN Ia

\* E-mail: michael.childress@anu.edu.au

DTD appears consistent with a  $t^{-1}$  power law (Totani et al. 2008; Maoz et al. 2011; Graur & Maoz 2013), such that the prompt SN Ia progenitors have a much higher representation than the old tardy progenitors (Förster et al. 2006).

The integrated rate of SNe Ia in a particular galaxy is the convolution of the SN Ia DTD with the star formation history (SFH) of the host galaxy (Yungelson & Livio 2000). The integrand of that convolution (i.e. the product of the DTD and the galaxy’s stellar age distribution) represents the likelihood function for the age of a given SN Ia in that galaxy. Equivalently, this represents the progenitor age distribution for a large sample of SNe Ia drawn from stellar populations with that mean SFH. To fully exploit the power of this progenitor age distribution requires a knowledge of galaxy SFHs, which are observationally challenging to constrain. Instead, we will show how knowledge of galaxy star formation rates (SFR) throughout cosmic time can constrain galaxy stellar mass assembly histories. These in turn can be coupled to an observationally-motivated SN Ia DTD to produce SN Ia progenitor age distributions at all galaxy mass scales and all redshifts.

In this work we focus on how SN Ia ages depend on the stellar mass of their host galaxies, from low-mass dwarf galaxies ( $\log(M_*/M_\odot) \sim 8$ ) to the most massive ( $\log(M_*/M_\odot) \sim 12$ ) ellipticals. Throughout this work, we refer to this as the “galaxy mass sequence”. The progression of SN Ia progenitor ages along the galaxy mass sequence, and its evolution with redshift, have critical implications for the use of SNe Ia as cosmological distance indicators. Observations of SNe Ia led to the discovery of the accelerating expansion of the Universe (Riess et al. 1998; Perlmutter et al. 1999) and continue to constrain cosmological parameters (e.g., Sullivan et al. 2011; Suzuki et al. 2012; Rest et al. 2013; Betoule et al. 2014). While systematic uncertainties had for a time constituted the dominant fraction of the SN Ia cosmology error budget (Scolnic et al. 2013, 2014; Betoule et al. 2013; Mosher et al. 2014), significant effort has been expended to reduce systematics so that statistical error now dominates the error budget (Betoule et al. 2014). This statistical error arises from the “intrinsic scatter” in corrected SN Ia luminosities, making the search for possible astrophysical drivers of this scatter of paramount importance.

More concerning is the recent discovery of a bias in the standardized SN Ia luminosities with the properties of their host galaxies. These luminosities, quantified by deviations from the best-fit cosmology on the Hubble Diagram (“Hubble residuals”), were found to depend on the mass (and/or metallicity) of their host galaxies (Sullivan et al. 2010; Kelly et al. 2010; Lampeitl et al. 2010; Gupta et al. 2011; D’Andrea et al. 2011; Konishi et al. 2011; Galbany et al. 2012; Hayden et al. 2013; Johansson et al. 2013; Childress et al. 2013). Childress et al. (2013) inspect the trend of Hubble residuals along the galaxy mass sequence and find age to be the physical property most consistent with the observed trend. Johansson et al. (2013) reach a similar conclusion. Furthermore, based on the analysis of SF intensity at SN Ia locations, Rigault et al. (2013, hereafter R13) find this host bias is most likely driven by fast declining SNe Ia in passive regions within their host galaxies (though these SNe Ia could cease to be problematic with the use of a properly

trained SN Ia light curve fitter, see e.g. Kim et al. 2013, 2014). These results indicate that progenitor age could impart a critical bias on the measurement of cosmological parameters with SNe Ia.

In Section 2 we describe our empirical model for the buildup of stellar mass in galaxies over cosmic time and in Section 3 we use this model to examine the progenitor age distribution of SNe Ia from  $z = 2$  to the present epoch. The mean ages of SNe Ia as a function of their host galaxy stellar mass is presented in Section 4. We then show that the trend of SN Ia age with host mass is robust against uncertainties in the stellar mass assembly history of galaxies (Section 5) or the exact form of the SN Ia DTD (Section 6). We summarize and conclude in Section 7. For the required calculation of lookback time as a function of redshift, we employ the standard “concordance”  $\Lambda$ CDM cosmology with  $\Omega_M = 0.30$ ,  $H_0 = 70 \text{ km s}^{-1} \text{ Mpc}^{-1}$ , and  $\Omega_\Lambda = 0.70$ .

## 2 THE STELLAR MASS DEPENDENCE OF GALAXY STAR FORMATION HISTORIES

Understanding the mass assembly and star formation history of galaxies over cosmic time is a rich and vigorous field of study (for a recent review see Madau & Dickinson 2014). In this Section we utilize observational constraints on star formation (SF), mass recycling, and SF quenching to forward model the buildup of stellar mass in galaxies over cosmic time. Specifically, we focus on the mean SFH of galaxies as a function of their stellar mass at all redshifts. The quantitative parametrizations of all galaxy scaling relations employed in our models are presented in full in Appendix A. This Section focuses on describing the qualitative features of our model, while the pertinent equations from Appendix A are referred to parenthetically for reference. We show later (Section 5) that the main results of this work are highly insensitive to the specific parametrizations employed for galaxy stellar mass assembly.

In the local Universe, the star formation rate is strongly correlated with the stellar mass (Salim et al. 2007; Elbaz et al. 2007) and similar trends are seen out to  $z \sim 2$  (e.g., Noeske et al. 2007; Pannella et al. 2009; Karim et al. 2011; Whitaker et al. 2012; Kashino et al. 2013; Zahid et al. 2012, Z12 hereafter). The slope and scatter of the relation between stellar mass and SFR is not strongly dependent on redshift (e.g., Z12; Noeske et al. 2007; Whitaker et al. 2012). These observations provide strong constraints for the stellar mass buildup of galaxies (e.g., Z12; Leitner 2012). For our stellar mass assembly tracks, we use the Z12 parametrization of the relationship between SFR, stellar mass, and redshift (hereafter the “SMz relation”).

Eventually galaxies use up (or perhaps lose) their gas which could be converted into stars, and star formation effectively ceases (or “quenches”). The mass functions of “active” star-forming galaxies and “passive” galaxies with little or no star formation (typically separated using color-magnitude diagrams) reach equality at  $z \sim 0$  at a mass scale of  $\log(M_*/M_\odot) \sim 10.0 - 10.4$ . This “quenching mass” has been measured in the local universe by GAMA (Baldry et al. 2012) and SDSS (Bell et al. 2003; Baldry et al. 2004); at intermediate ( $z \lesssim 2$ ) redshifts by deep surveys such as COMBO-17 (Borch et al. 2006), DEEP2 (Bundy et al.

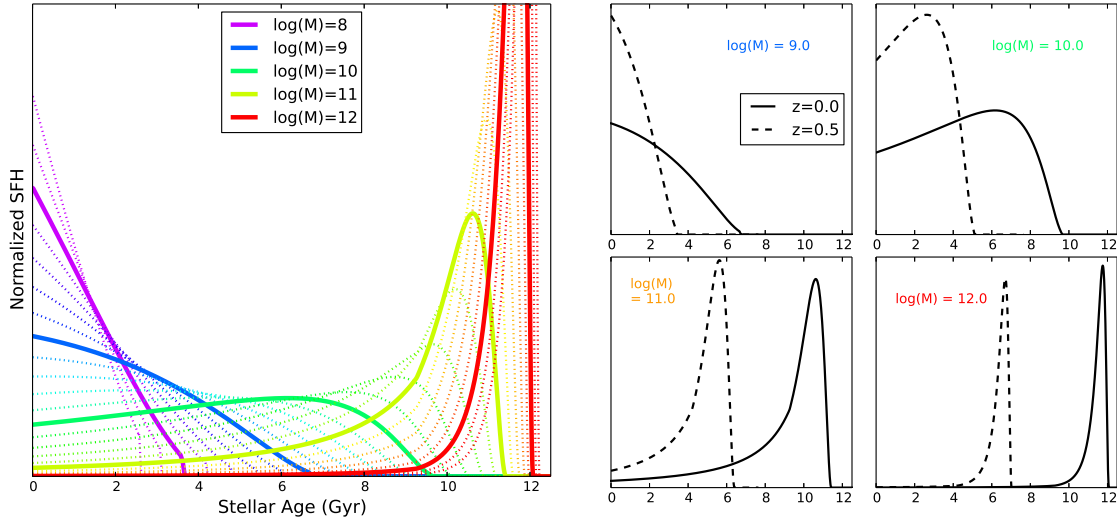


**Figure 1.** *Left:* Final mean SFHs along the galaxy mass sequence for our models, in steps of 0.1 dex from  $\log(M_*/M_\odot) = 7.5$  to  $\log(M_*/M_\odot) = 12.5$ . Integer log stellar mass values are highlighted as thick solid curves. *Right:* Mean SFHs at the current epoch ( $z = 0$ ) and at the same mass scale 5 Gyr in the past ( $z = 0.5$ ) for select final stellar mass values.

2006), and NEWFIRM (Brammer et al. 2011); and more recently at very high redshifts ( $2 \lesssim z \lesssim 4$ ) with the COSMOS/UltraVISTA survey (Muzzin et al. 2013). The dependence of this quenching mass with redshift has been fit by Muzzin et al. (2013), and we use this redshift dependence (Equation A3) in our baseline mass assembly models.

The quenching mass scale in Equation A3 represents the *median* quenching mass, when active and passive galaxies are equally represented. For our models we require a prescription for the passive galaxy fraction as a function of galaxy stellar mass. This can be explicitly calculated when the Schechter function parameters for active and passive galaxies are well-measured, but is challenging when these are poorly constrained. Using the blue and red galaxy mass functions at low redshift ( $z = 0.1$ ) where the active and passive Schechter function parameters are well measured from Moustakas et al. (2013), we find the passive fraction is accurately represented by an error function centered at the median quenching mass and with a width of 1.5 dex in log stellar mass (Equation A4). To simplify the modeling process, we thus adopt this functional form for all redshifts with a redshift-dependent median quenching mass that follows Equation A3.

We note, however, that the quenching mass scale derived from color-based separation of active and passive galaxies are likely to be slightly biased to lower values. This is due to the high-mass end of the star-forming main sequence having some overlap with (and thus contaminating) the red galaxy sequence due to the combination of its low sSFR and reddening by dust. Dust reddening is also higher in high-mass star-forming galaxies (e.g. Lee et al. 2009; Garn & Best 2010; Zahid et al. 2013a,b), hence a significant tail of the SF galaxy population is likely to be wrongly attributed to the quenched population (e.g. Wolf et al. 2009). This effect was first noticed in galaxy clusters (Wolf et al. 2005) but extends to field galaxy samples as well. As a requisite example, Spitler et al. (2014) used multi-band SEDs for

$z \sim 3-4$  galaxies from the ZFOURGE survey to cleanly separate dusty and truly passive galaxies, and found that dusty star-forming galaxies may constitute nearly half of red massive galaxies (see also Straatman et al. 2014). Moreover, the intrinsic color distributions of active and quiescent galaxies have some overlap and thus cannot be separated without contamination using a strict color cut (Taylor et al. 2014). We will revisit these concerns and their (negligible) implications for our conclusions in Section 5.

The calculation of a galaxy’s integrated SFH must also take into account the fraction of gas converted into stars that will be recycled back to the interstellar medium (ISM) by supernovae or stellar winds. This recycling fraction depends on time because lower mass stars progressively evolve off the main-sequence and also depends on the stellar initial mass function (IMF). Leitner & Kravtsov (2011) explored these effects in detail, and found that the fraction of material returned to the ISM rises rapidly in the first few Gyr, and then levels off. They found that the fraction of stellar mass returned to the ISM from a single burst of SF could be well parametrized by a shifted exponential function (Equation A2). For our analytical galaxy SFHs, we utilize this functional form along with the parameters derived by Leitner & Kravtsov (2011) for a Chabrier (2003) IMF.

The above prescriptions provide the critical pieces necessary to model the buildup of stellar mass in galaxies:

- (i) The dependence of SFR on current stellar mass and its evolution in redshift (Equation A1).
- (ii) The fraction of stellar mass returned to the ISM as a function of time (Equation A2).
- (iii) The stellar mass scale at which star formation ceases, and its dependence on redshift (Equation A3).
- (iv) The fraction of galaxies which have ceased SF as a function of stellar mass (Equation A4).

With these we can construct galaxy SFHs by integrating a galaxy’s SFR over cosmic time (Equation A5). Such a pro-

cedure was explored in detail in Z12, and we adopt a similar but slightly modified technique for deriving analytical galaxy SFHs along the galaxy mass sequence. In practice, we begin with a set of mass evolution tracks starting from a mass of  $M_* = 10^6 M_\odot$  at some time of formation  $t_F$  then follow the SMz relation to the present epoch  $z = 0$ . We model tracks with various values of  $t_F$  (in steps of 50 Myr from 1-10 Gyr, and steps of 25 Myr from 10-13 Gyr of lookback time), and forward model the mass buildup with time steps of 0.5 Myr.

To obtain the SFH for galaxies of a given stellar mass, we must account for the effects of SF quenching. For this, we impose a “quenching penalty” on the SF of our model galaxies at each time step by multiplying the SF from the SMz by the passive galaxy fraction at the current galaxy mass scale at the epoch of that time step (see Equation A5).

The final SFHs from our models are shown in Figure 1 in steps of 0.2 dex from  $\log(M_*/M_\odot) = 7.6$  to  $\log(M_*/M_\odot) = 12.4$ . The right panels of this Figure show SFHs for several specific stellar mass values at both the current epoch ( $z = 0$ ) and 5 Gyr in the past ( $z = 0.5$ ). For higher mass galaxies, the mean SFHs generally are confined to a small distribution of old ages, reflecting the rapid transition to fully quenched SF. Lower mass galaxies tend to be almost completely unquenched, and generally show SFRs that increase toward the current epoch.

The SFR-mass trend, effects of SF quenching, and their respective evolutions in redshift, combine to paint a picture of SFHs along the galaxy mass sequence. Massive galaxies above the quenching mass at a given epoch formed the majority of their stars 5-10 Gyr in the past and effectively ceased SF at high redshift ( $z \gtrsim 2$ ), while less massive galaxies ( $\log(M_*/M_\odot) \lesssim 10$ ) formed more of their stars recently and indeed are still actively forming stars. The quenching epoch for massive galaxies is at roughly 10 Gyr in the past for massive  $z = 0$  galaxies and at 5 Gyr in the past for massive  $z = 0.5$  galaxies. This will result in important consequences for the mean progenitor ages for SNe Ia along the galaxy mass sequence, as we explore below in Section 4.

Though our models by construction obey the SMz relation and quenching fraction at all redshifts, it is worthwhile to confirm that they paint a consistent picture for the global SFH of the Universe. We therefore calculate our prediction for the SFH of the Universe by summing our mean SFHs weighted by the total stellar mass in each logarithmic galaxy mass bin at  $z=0$ . This is simply a modified Schechter function, for which we use the Moustakas et al. (2013) data (which we find is well-fitted by a double Schechter function with parameters  $\alpha_1 = -1.42$ ,  $\log M_1^* = 11.12$ ,  $\phi_1^* = 1.39 \times 10^{-3}$ ,  $\alpha_2 = -0.45$ ,  $\log M_2^* = 10.66$ ,  $\phi_2^* = 6.57 \times 10^{-3}$ ).

In Figure 2 we show our model’s prediction for the cosmic SFH at  $z = 0$  compared to that derived from the compilation of observational data in Behroozi et al. (2013, hereafter B13). As with the observed CSFH, our prediction for the CSFH shows a characteristic peak near  $z \sim 2$ , and declines toward the present epoch. Some discrepancy is evident here, and we show in Section 5 that these differences can be reconciled with some adjustments to the galaxy mass assembly models. It is worth noting that accurate prediction of the cosmic SFH is still a challenge for the galaxy evolution community, even with simulations that fully track dark matter structure growth (e.g., Springel et al. 2005) with added

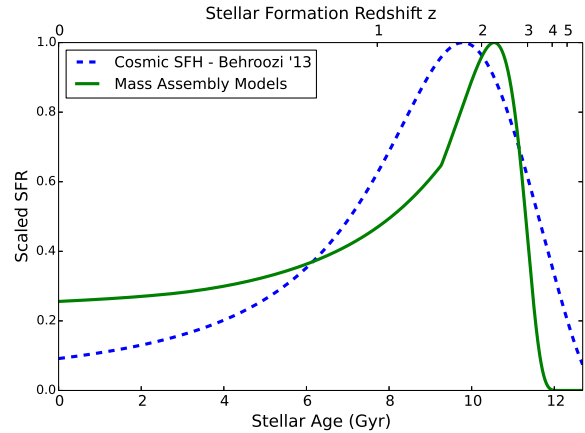


**Figure 2.** Predictions for the volume-averaged star formation history of the Universe obtained from the Schechter function-weighted sum of our mass assembly models (solid green curve) compared to the cosmic SFH inferred from the compilation of SFR data presented in Behroozi et al. (2013).

prescriptions for baryonic physics. Our CSFH is produced solely from the mass-dependent galaxy SFHs from our models weighted by the observed number density of galaxies as a function of mass in the local Universe. That we obtain the level of qualitative agreement seen here is encouraging for the validity of our galaxy SFHs. Most importantly, in Section 5 we show that any attempted adjustments to our mass assembly models cannot negate our conclusions regarding SN Ia ages and their relationship with host galaxy mass throughout cosmic time.

### 3 THE DISTRIBUTION OF SN Ia AGES OVER COSMIC TIME

In this section we use our empirical galaxy SFHs from Section 2 to infer the SN Ia progenitor age distribution as a function of host galaxy mass and redshift. We begin by inspecting the SN Ia age distribution in individual galaxies in Section 3.1. In Section 3.2 we show how SN Ia progenitor age distributions across the galaxy mass sequence manifest a sharp bimodality in the global SN Ia progenitor age distribution. Finally in Section 3.3 we inspect how the SN Ia progenitor age distribution evolves in redshift.

#### 3.1 SN Ia Age Distribution for a Single Galaxy

The rate of SNe Ia in a galaxy at a specific epoch  $t_0$  is the convolution of the SN Ia DTD  $\phi(\tau)$  with the galaxy SFH  $\psi(\tau)$ :

$$R(t_0) = \int_0^\infty \phi(\tau) \psi(t_0 - \tau) d\tau \quad (1)$$

While Equation 1 gives the total integrated SN Ia rate in a given galaxy, the integrand is in fact the probability distribution for the age of the progenitor system for any SN Ia occurring in that galaxy:

$$P(\tau; t_0) = \phi(\tau) \psi(t_0 - \tau). \quad (2)$$

When  $\tau > t_0$ ,  $\psi = 0$ . Thus  $P(\tau; t_0)$  is the likelihood at epoch  $t_0$  of the SN arising from a progenitor system of age  $\tau$ , and  $\psi(t_0 - \tau)$  is effectively the age distribution of all stars in the parent galaxy (if one corrects for the stellar mass lost over time). The quantity  $P(\tau; t_0)$  also represents the *age distribution* for a large sample of SNe Ia arising from the same galaxy, or equivalently from many galaxies with the same SFH. Thus, the mean SFHs calculated in Section 2 are appropriate for calculating the age distribution for many SNe Ia occurring in host galaxies with the same stellar mass.

In order to avoid sharp features in the SN Ia age distribution, we adopt a smooth functional form for our “nominal” SN Ia DTD as follows:

$$\phi(t) \propto \frac{(t/t_p)^\alpha}{(t/t_p)^{\alpha-s} + 1} \quad (3)$$

At late times ( $t \geq t_p$ ), this function form rapidly approaches a  $t^s$  power law, with observations favoring a power law slope for the SN Ia DTD of  $s = -1$ . At early times ( $t \leq t_p$ ) this function is a high order ( $\alpha$ ) polynomial which flattens to zero rapidly below some characteristic “prompt” timescale ( $t_p$ ). This functional form for the SN Ia DTD is of course entirely artificial, but reflects the qualitative traits inferred from observations. We will show in Section 6 that our primary results are insensitive to the exact form of the DTD, but instead are driven very strongly by the steep ( $\sim t^{-1}$ ) slope of the DTD. We adopt a fiducial DTD with  $s = -1$  and  $t_p = 0.3$  Gyr for the main analyses of this paper.

In Figure 3 we show the age distribution calculated by convolving our smooth DTD function (Equation 3) with the mean SFHs from Section 2 for several values of stellar mass. The bottom right summary panel of this figure compares the SN Ia age distributions for the various host masses, and illustrates one of the key results of this paper: *in galaxies that are actively star-forming, the SN Ia age distribution is shaped more strongly by the shape of the DTD than by that of its host galaxy SFH*. For the three example galaxies in Figure 3 whose SFH has strong recent star formation, the SN Ia age distributions all peak at the same age where the DTD peaks. This is because the evolution of SFR in these galaxies is much more gradual than the steep decline in SN Ia rates as a function of stellar age.

The two example galaxies in Figure 3 with SFH dominated by an old stellar population exhibit a markedly different SN Ia age distribution. In these examples, the galaxies rapidly form a large mass of stars over a short duration ( $\sim 1$  Gyr) at a distant past epoch ( $\sim 8-10$  Gyr). Here the resultant SN Ia age distribution mimics the stellar age distribution (note that  $t/\Delta t$  is large so the  $t^{-1}$  DTD does not significantly alter the shape of the host stellar age distribution). We note that for galaxies with even a small amount of recent star formation ( $\log(M_*/M_\odot) = 11$  in Figure 3), a non-negligible component of the SN Ia age distribution appears at the DTD peak. However, the second major conclusion of this work holds true: *in galaxies dominated by old stellar populations, the mean SN Ia age traces the mean epoch when the stellar mass was formed*.

### 3.2 The Bimodality of SN Ia Ages

With our galaxy mass assembly models in hand and a chosen SN Ia DTD, we can calculate the intrinsic distribution

of progenitor ages for SNe Ia occurring in the local (and distant) Universe. We previously calculated the average (normalized) SFH as a function of galaxy stellar mass, which we plot in two-dimensional age-mass parameter space in the left panel of Figure 4. Convolved with our nominal SN Ia DTD (Eq. 3), this produces the relative age distributions, which we show in age-mass space in the middle panel of Figure 4 (note these are *not* re-normalized).

Finally, to obtain the intrinsic distribution of SNe Ia in age-mass space, we need to account for the volume density of total stellar mass in each logarithmic galaxy mass bin. Again, this is simply a modified Schechter function, for which we use the low redshift values from Moustakas et al. (2013) as previously noted. The final number density of SNe Ia in progenitor age-host mass space is shown in the right panel of Figure 4.

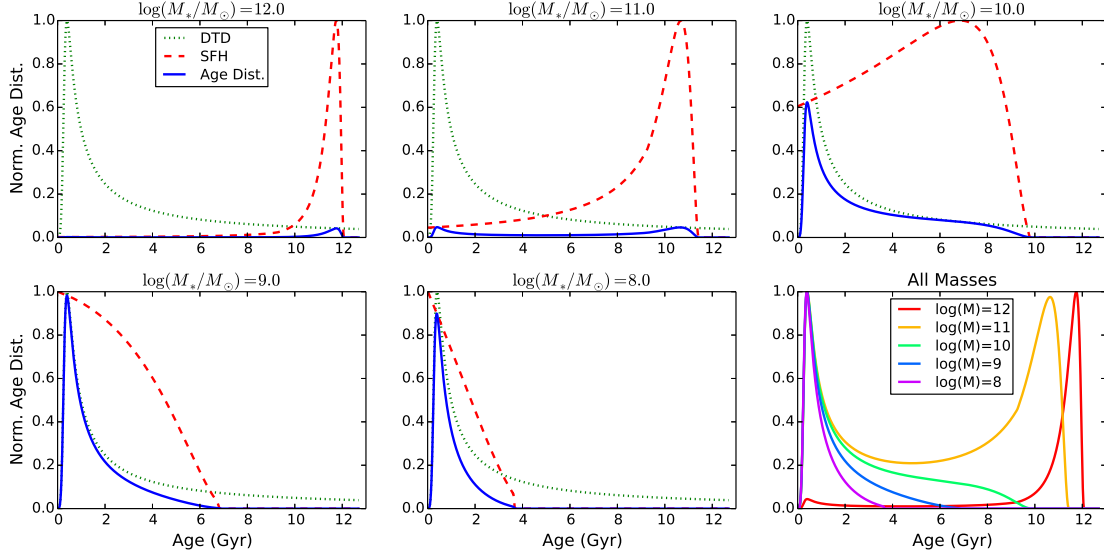
The age distribution of SNe Ia in Figure 4 shows a striking existence of two primary modes. The young component of this distribution, commonly referred to as the “prompt” component in the literature, is dominant at low stellar mass and exhibits the same peak age in all actively star-forming galaxies. The old component, often called the “tardy” component, forms a subdominant component at old stellar ages almost exclusively in high-mass galaxies.

Figure 4 also naturally explains why the SN Ia rate has been so well parametrized by the two-component (or “A+B”) model, with one component of the rate proportional to galaxy stellar mass (“A”) and another proportional to its SFR (“B”). Massive galaxies formed their stars during a short period in the distant past, so the relative SN Ia rate (corresponding to the DTD at that age) depends on the total stellar mass of the galaxy since all the stellar mass was formed at a similar epoch. Actively star-forming galaxies (regardless of their detailed SFH) are dominated by the DTD peak age, which closely tracks the recent galaxy SFR.

Because our galaxy mass assembly models are tracked self-consistently from high redshift, we can inspect the SFHs of galaxies of any stellar mass at any redshift. This allows us to inspect how the age distribution of SN Ia ages evolves over cosmic time. As an example, we recalculate the mean SFHs for galaxies at redshift  $z = 0.5$ , and use the Schechter function parameters at that redshift (the sum of the blue and red galaxy mass functions fits from Borch et al. 2006), to derive the SN Ia distribution in age-mass space at  $z = 0.5$ . We show this  $z = 0.5$  age distribution as the thick contours in Figure 5, compared to the  $z = 0.0$  distribution (density plot and thin red contours).

Several key features are evident from this result. First, the bimodality of SN Ia ages persists even at high redshift, due to the nature of galaxy SFHs generally corresponding to either current active star formation or quenched past star formation. Next, the SFHs of star-forming galaxies at high redshift are again shallow compared to the  $t^{-1}$  SN Ia DTD, meaning the prompt SN Ia component again arises predominantly from the age of the DTD peak. This held true at every redshift we calculated, implying the critical result *young (prompt) SNe Ia arise from the same uniform progenitor age group throughout cosmic history*.

Finally, critical contrast is seen for the old (tardy) SN Ia component. Though the old component again arises from the past epoch when star formation occurred rapidly and then ceased in massive galaxies, this occurred at a different past



**Figure 3.** SN Ia age distributions (solid blue curve in the first five panels) calculated as the integrand of the convolution of the SN Ia DTD (dotted green curve) and galaxy SFH from our empirical models (dashed red curve). The SFHs have been plotted over lookback time to reflect the convolution step, and the age distribution is the product of the DTD and SFH. The bottom right panel shows the peak-normalized age distribution for the chosen galaxy mass scales presented in the first five panels.

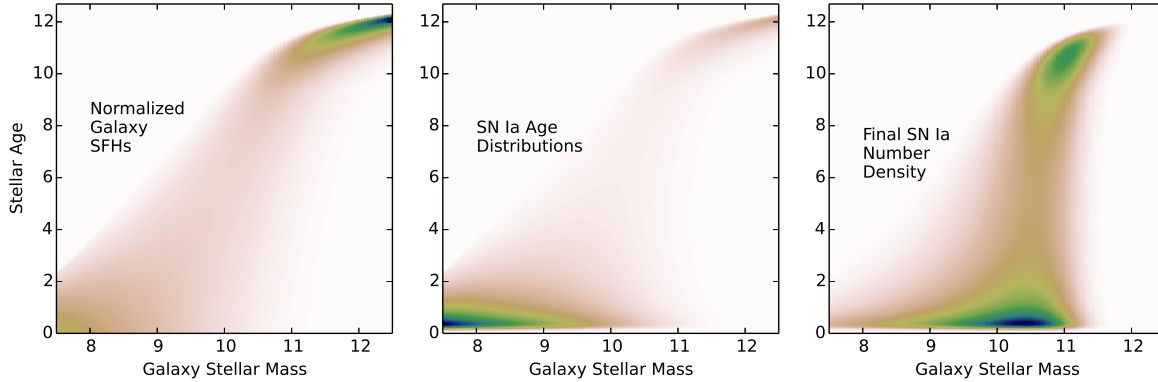


**Figure 4.** *Left:* Normalized mean galaxy SFHs as a function of total stellar mass. *Middle:* SN Ia age distribution versus host galaxy mass (not re-normalized: age distribution per unit mass). *Right:* Intrinsic distribution of SNe Ia in progenitor age-host mass space in the local Universe ( $z = 0$ ).

age for  $z = 0.5$  galaxies than for  $z = 0.0$  galaxies. This means the *old SNe Ia arise from different progenitor ages at different redshifts*. Thus, SNe Ia in passive galaxies present a diverse and evolving progenitor age group over cosmic history, while young SNe Ia from actively star-forming galaxies remain highly uniform in their progenitor ages at all cosmic epochs.

As an additional cross-check against data, we show in the lower panel of Figure 5 the prediction of our fiducial models for the SN Ia host galaxy mass distribution compared to that observed at low redshift by PTF (Pan et al. 2014). The shapes of the predicted and observed distributions are modestly consistent, but with a mild over-prediction of high-mass hosts. We will show in future work (Childress & SNfac-

tory, in prep.) that the shape of this host mass distribution can actually *constrain* the SN Ia DTD.

### 3.3 Evolution of the SN Ia Age Distribution

Following the same procedure for calculating the SN Ia age distribution in a single galaxy, we can couple our DTD to the cosmic SFH (again from B13) to calculate the global SN Ia age distribution at a given redshift. This age distribution can also be calculated by integrating the SN Ia age distribution as a function of galaxy mass, weighted by the modified Schechter-function (i.e., the right panel of Figure 4). However, as we showed in Figure 2, our baseline models do not exactly match the observed CSFH (though see Section 5.4),



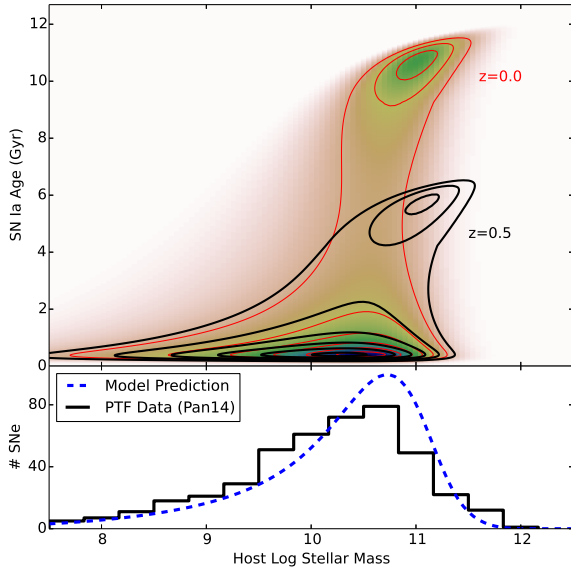


**Figure 5.** Top: Same as right panel of Figure 4, but with contours drawn for both  $z = 0.0$  (thin red) and  $z = 0.5$  (thick black). Bottom: SN Ia host galaxy mass distribution as predicted by our models at  $z = 0$  (blue curve) compared to data (black histogram) from PTF (Pan et al. 2014).

so we prefer the B13 CSFH for calculating the aggregate SN Ia age distribution.

Note this the SN Ia age distribution is a different quantity than the delay time distribution, which reflects the intrinsic progenitor age distribution for all SNe Ia produced by a single burst of star formation, counted over all epochs following the SF burst. The age distribution we discuss here is the distribution of progenitor ages which give rise to the sample of SNe Ia occurring at a single epoch of cosmic time, summed over all galaxies in a large homogeneous volume of space (note this age distribution *can* take the same form as the DTD if produced from galaxies having a constant SFR for infinite duration).

In Figure 6 we present this age distribution for SNe Ia at various redshifts from  $z = 0.0$  to  $z = 2.0$ . The age distributions in Figure 6 exhibit several important features. First, the bimodality of SN Ia ages is evident up to redshift  $z = 0.5$ , but the mean age of the old (tardy) component decreases at higher redshift and eventually the two components become blended. Second, the prominence of the tardy peak decreases with redshift, but not so extremely as expected from “A+B” rate calculations coupled to the evolution of the cosmic star formation rate. Using the  $z = 0$  “A” and “B” coefficients would imply that the fraction of old (tardy) SNe Ia drops by a significant factor by redshift  $z = 0.5$  (Sullivan et al. 2006; Howell et al. 2007), but the younger age of the high-redshift tardy component results in a higher rate than the “A+B” calculation due to the  $t^{-1}$  DTD. This critical result implies that *the old (tardy) component of SNe Ia comprises a non-negligible fraction of SNe Ia at the redshifts ( $z \sim 0.5$ ) of existing major cosmological SN Ia samples.*

As a further consistency check, we can predict the evolution of the integrated SN Ia rate with redshift using our galaxy mass assembly models. In the lower panel

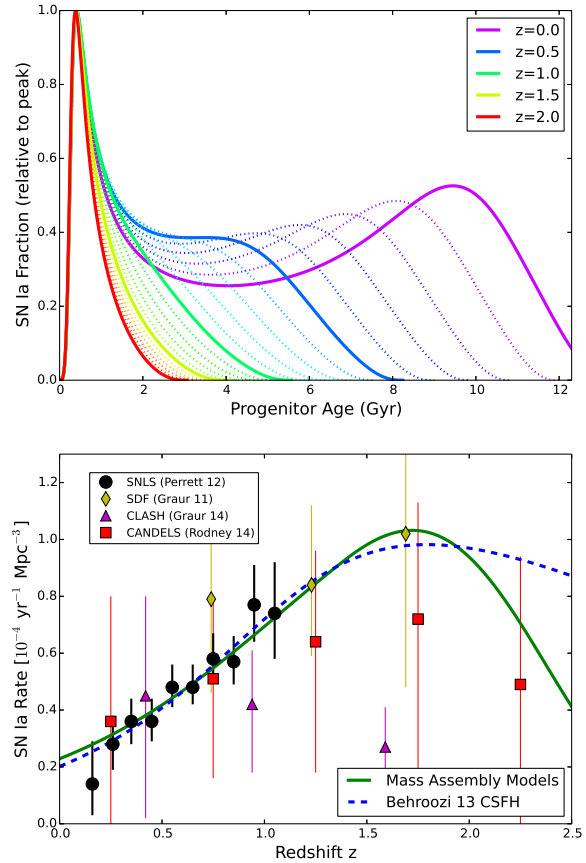


**Figure 6.** Top: Intrinsic SN Ia age distribution as a function of redshift from  $z = 0.0$  (purple) to  $z = 2.0$  (red) in steps of 0.1 (dotted lines), with half-integer redshift steps denoted as thick solid lines. Based on convolution of the B13 CSFH with our smooth DTD (Equation 3). Bottom: Predicted evolution of the SN Ia rate with redshift for our mass assembly models (solid green curve) and the B13 CSFH (dashed blue curve) compared to data from SNLS (Perrett et al. 2012), Subaru Deep Field (SDF; Graur et al. 2011), CLASH (Graur et al. 2014), CANDELS (Rodney et al. 2014).

of Figure 6, we plot the prediction of our models for the SN Ia rate as a function of redshift, as well as the prediction for the observed CSFH from B13. These predicted rates are compared to observations from several key recent SN Ia rates studies from major surveys: the Supernova Legacy Survey (SNLS; Perrett et al. 2012), the Subaru Deep Field (SDF; Graur et al. 2011), and CLASH survey (Graur & Maoz 2013), and the CANDELS survey (Rodney et al. 2014). Both models are normalized to the SNLS (Perrett et al. 2012) rate data, and show good agreement with the redshift evolution of the SN Ia rates from this precise analysis.

#### 4 SN Ia AGES ALONG THE GALAXY MASS SEQUENCE

In addition to calculating the aggregate SN Ia progenitor age distribution across all galaxies, we can examine how the

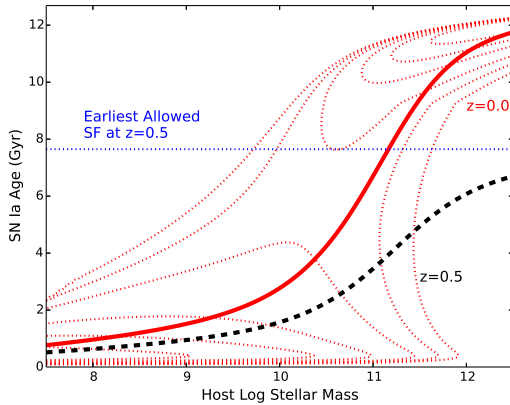


**Figure 7.** Mean age of SNe Ia as a function of host galaxy mass at redshift  $z = 0$  (solid red curve) and  $z = 0.5$  (dashed black curve). For reference, we show the SN Ia age distribution at  $z = 0$  as the dotted red contours (normalized at each galaxy mass value), as well as the earliest epoch of allow star formation at  $z = 0.5$  (dotted blue line).

SN Ia age distributions of Section 3 vary as a function of host galaxy stellar mass. In Figure 7, we plot the mean of the SN Ia age distribution as a function of host galaxy stellar mass both in the local ( $z = 0.0$ ) and distant ( $z = 0.5$ ) Universe.

From Figure 7 we see a clear trend of SN Ia age with host galaxy mass that broadly reflects the behavior identified from SN Ia age distributions of individual galaxies in Section 3.1. Low-mass galaxies are actively star-forming, and thus have SN Ia age distributions strongly dominated by younger progenitor populations. In contrast, high-mass galaxies formed most of their stars in the distant past, so the SNe Ia they produce are consistently old. The age-mass trend shows a rapid transition between  $10.0 \leq \log(M_*/M_\odot) \leq 11.5$  as galaxies are influenced and then dominated by quenching. This age transition resembles the step-like structure of the SN Ia Hubble residual trend with host galaxy mass, as identified by C13 and Johansson et al. (2013).

As an additional consistency check, we take advantage of the fact that our models predict the mean age of galaxies as a function of their stellar mass. Host galaxy age is also known to tightly correlate with SN Ia stretch (Howell et al. 2009; Neill et al. 2009; Johansson et al. 2013), allowing us to predict the mean stretch of SNe Ia versus host galaxy mass. In Figure 8 we show the stretch (here SALT2  $x1$ ) versus mass data from SNLS (Howell et al. 2009; Sullivan et al. 2010), both as individual SNe and in bins of 0.5 dex in host mass. To this we compare the prediction for  $x1$  versus host mass using the  $x1$ -age (note here this is mean host galaxy age, not the age of the SN) slope from Johansson et al. (2013) with a zeropoint that best fits the data. This model shows surprisingly good agreement with the observed evolution of  $x1$  with host mass, lending support to our galaxy mass assembly models.

Our results for mean SN Ia age versus host mass support the suggestion by C13 that the step-like shape of the SN Ia Hubble residual trend with mass is driven by progen-

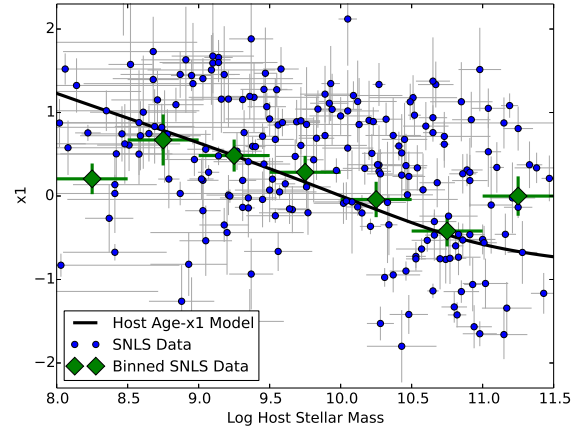


**Figure 8.** Observed SN Ia stretch (here SALT2  $x1$ ) versus host galaxy mass for the SNLS (Howell et al. 2009; Sullivan et al. 2010) sample, both as individual objects (blue points) and binned averages (green diamonds) in bins of 0.5 dex in host stellar mass. To this we compare the prediction for mean  $x1$  versus host mass using the relationship between SN Ia stretch and host galaxy age (Johansson et al. 2013) coupled to our galaxy mass assembly models.

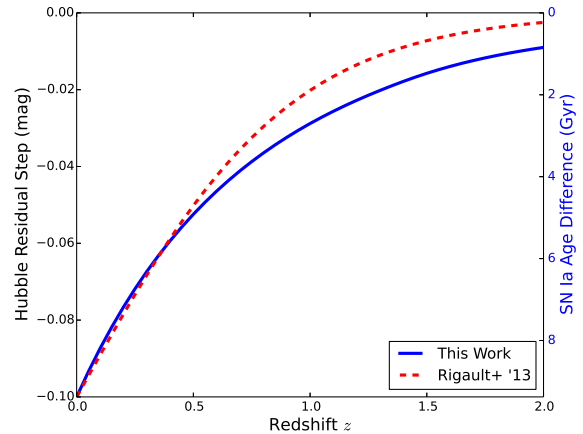


**Figure 9.** Evolution of the SN Ia Hubble residual (HR) “mass step” value with redshift, from our SFH models (solid blue curve) and using Equations (5) and (6) from Rigault et al. (2013). For illustrative purposes, we set the HR step to -0.10 mag at  $z = 0$ , and scale this value by the mean age difference between high and low-mass bins (split at  $\log(M_*/M_\odot) = 10$ ).

itor age. The evolution of galaxy populations over cosmic time implies this age-mass trend will also evolve with redshift. In Figure 7, we also show the SN Ia mean age trend with host galaxy mass at  $z = 0.5$ , clearly illustrating this effect

To quantify the evolution of the SN Ia age-mass trend and the resulting Hubble residual step in host mass (hereafter, the “HR step”), we calculate the mean SFH for galaxies at the same mass sampling as above, for all redshifts between  $z = 0$  and  $z = 2$  in steps of  $\Delta z = 0.05$ . At each redshift, we calculate the difference between mean age in the high-mass bin (defined by  $\log(M_*/M_\odot) \geq 10$ ) and low-mass



bin. We find the age difference between mean SN Ia age at  $\log(M_*/M_\odot) = 12$  and  $\log(M_*/M_\odot) = 8$  scale similarly to this binned age difference. We also find that the galaxy mass scale at which mean SN Ia age was halfway between the high- and low-mass values (i.e. the “transition” mass) was consistent to within 0.1 dex across all redshifts.

We examine the evolution of the HR step with redshift under the scenario where it is proportional to age differences. In Figure 9 we plot the HR step versus redshift assuming the  $z = 0$  value is -0.10 mag. We see that the HR step decreases significantly at high redshifts. Similarly, R13 find that the HR step appeared to be driven by SNe Ia in passive environments in high-mass hosts, and calculated the HR step evolution with redshift assuming it scales with the cosmic sSFR. We show the results of the R13 model in Figure 9 compared to ours, and they appear quite similar. One distinct difference is that the R13 model predicts the HR step is nearly zero at  $z = 2$ , while our models still exhibit a nonzero value. This is due to our models tracking the diminishing, but non-vanishing, age difference between the prompt SN Ia timescale (set consistently by the DTD peak) and the tardy SN Ia timescale (set by the evolving stellar ages in massive galaxies).

## 5 SN Ia AGES: SENSITIVITY TO GALAXY SFHS

The buildup of stellar mass in galaxies is a rich field of study, and a full census of possible approaches to modeling galaxy mass assembly is beyond the scope of this work. Instead, we are concerned with how variations in the nature of our mass assembly models affect the ages of SNe Ia. Our models were used to describe how the age distribution of stars in the local Universe is distributed along the galaxy mass sequence, which allows us to calculate the trend of SN Ia ages with host galaxy mass (Section 4). In this Section we will thus examine how subtly different parametrizations of galaxy mass assembly affect the SN Ia progenitor age-host mass trend.

As an additional diagnostic to test the reliability of the varied mass assembly models presented in this Section, we test the predicted cosmic SFH (CSFH) for each model against the observed CSFH (as in Figure 2). In the top panels of Figure 10 we show the predicted CSFH for each model variation compared to the observed CSFH of B13. The bottom panels of Figure 10 show the SN Ia age versus host mass trend predicted by the model variations. Section 5.1 presents variations to the galaxy SF quenching prescription, Section 5.2 discusses the effect of an SMz relation which gradually plateaus at high redshift, while Section 5.3 examines the possible impact of galaxy mergers. A “fine-tuned” model incorporating multiple adjustments is presented in Section 5.4, while a summary of all the model variations is presented in Section 5.5. The equations for the modified parametrizations employed in this Section are presented in Appendix A.

### 5.1 Variation in SF Quenching

Quenching of galaxy star formation is perhaps the most uncertain property of galaxy evolution incorporated into our

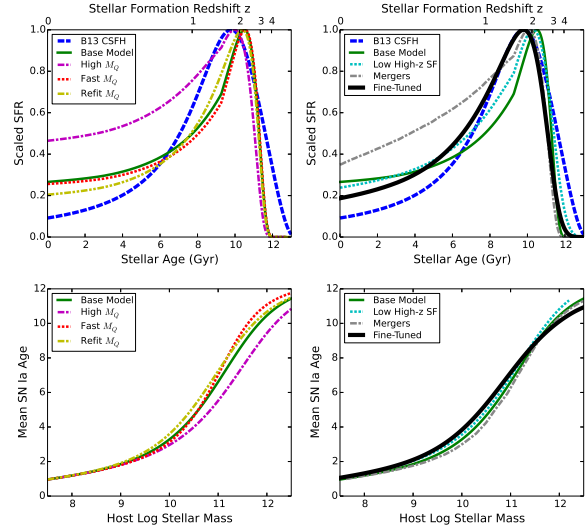


**Figure 10.** Top panels: Cosmic SFH predicted by each variation of our mass assembly models compared to the observed cosmic SFH from Behroozi et al. (2013). Bottom panels: SN Ia age versus host mass trend at  $z = 0$  for each variation of the mass assembly models. Note that even mass assembly modifications that produce seemingly major changes to the CSFH ultimately produce minor changes to the SN Ia age versus host mass trend.

models. The observational distinction between active and passive galaxies is typically performed with broad-band photometric colors, but by necessity this technique typically probes different rest wavelengths at different redshifts. As a result, several possible variations to the true quenching of galaxy SF could be possible, and we examine several of those here.

*Underestimated Quenching Masses?* First we consider whether the quenching mass scale estimated from photometric colors may not correspond directly to the epoch when SF ceases. Specifically, we investigate whether the true quenching mass may be underestimated by some amount. In the left panels of Figure 10 we present the results of repeating our galaxy mass assembly procedure, but with a quenching mass scale that is 0.5 dex higher than the Muzzin et al. (2013) parametrization employed in our nominal models. The result shows that the recent SF in the Universe is increased, since  $L^*$  galaxies (which contribute the most to SF at  $z < 1$  in our models) are not penalized for quenching. For SN Ia ages, this effect slightly raises the transition mass scale for SN Ia ages, but the clear age transition with host mass is robustly maintained.

*Faster Transition To Quenched?* Next we examine the effect of shortening the galaxy mass scale over which galaxies transition from active to passive. In our nominal models this was 1.5 dex, and in Figure 10 we present the results of reducing this to 1.1 dex (closer to the value implied from the GAMA mass functions of Baldry et al. 2012). This has an almost negligible effect on the predicted CSFH, and merely causes the SN Ia age-mass transition to occur on a proportionally shorter mass scale.

*Different  $M_Q(z)$  Parametrization?* Finally, we test the effect of employing a different parametrization for the quenching mass as a function of redshift  $M_Q(z)$ . We use

the Muzzin et al. (2013) data points up to redshift  $z = 2$ , along with the  $z = 0.06$  value for GAMA from Baldry et al. (2012), as well as the  $z \leq 2$  values from the ZFOURGE survey mass functions from Tomczak et al. (2014). We find these data were consistent with a linear functional form for  $M_Q(z)$ , resulting in a generally lower quenching mass below  $z \leq 1$  than that predicted in the Muzzin et al. (2013) parametrization. The CSFH below  $z \leq 1$  in turn shows better agreement with the observed CSFH from B13, and the SN Ia age-mass trend is virtually unchanged.

## 5.2 Impact of High- $z$ SF Intensity

The SMz relation we employ is based on the Z12 parametrization which describes observed data very well up to  $z \sim 2$ . However, our extrapolation of this relation beyond  $z = 2$  results in very intense high redshift SF (since the Z12 parametrization increases monotonically with redshift). Consequently, massive galaxies in our models form the majority of their stars in an extremely rapid period of time at high redshift, as they rapidly reach the quenching mass. This results in a narrow time scale for the formation of most of the Universe’s stellar mass in our models, seen as the narrowness of our model CSFH compared to the B13 data.

To examine a possible remedy to this situation, we construct an alternate model for the redshift evolution of the SMz relation while retaining the Z12 mass dependence. Our alternate parametrization (whose formulae are presented in Appendix A) is tuned to mimic the Z12 redshift dependence below  $z = 2$ , but to have a gentler redshift dependence above this redshift. This slowing of the high-redshift evolution of the SMz relation is observationally motivated by a slower evolution of galaxy SFRs above redshift  $z = 2$  (Stark et al. 2013). The resulting models present a CSFH which is broader in age (top right panel of Figure 10), and thus closer to the observed CSFH. The SN Ia age-mass trend retains its previously noted qualitative characteristics.

## 5.3 The Effect of Galaxy Mergers

The galaxy mass assembly models we have presented thus far assume that galaxies undergo secular evolution, where a single galaxy evolves independently of every other galaxy in the Universe. This neglects the observational fact that galaxies often undergo mergers, and this could contribute significantly to the buildup of stellar mass in galaxies especially since  $z = 1$  as the CSFH continuously declines (Bell et al. 2006; Conselice et al. 2008; de Ravel et al. 2009), particularly along the red sequence (Faber et al. 2007). Indeed, recent work from the GAMA survey (Robotham et al. 2014) has shown that while star-formation dominates stellar mass assembly at low galaxy mass scales (less than  $\log(M_*/M_\odot) \sim 10.6$ ), mergers represent the dominant mode through which massive galaxies continue to build their stellar mass.

The exact contribution of mergers to galaxy mass assembly is observationally difficult to constrain, and has only been examined across all galaxy mass scales in the local Universe (Robotham et al. 2014). Estimating merger rates is further complicated by the necessity to combine the volumetric merger fraction measured from a snapshot of some

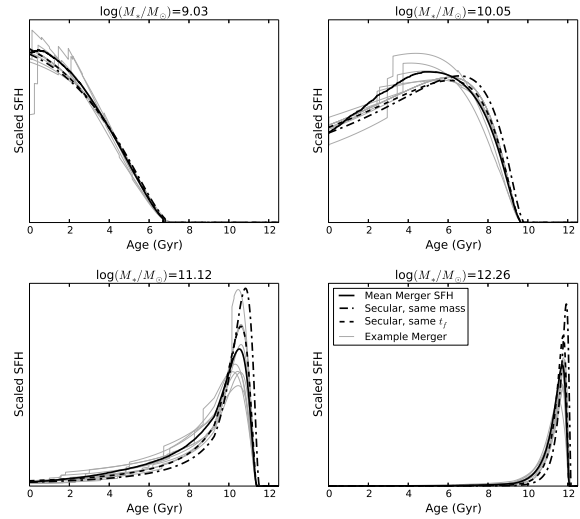


**Figure 11.** Mass assembly models incorporating mergers for four fixed formation times corresponding to  $\log(M_*/M_\odot) = 9, 10, 11, 12M_\odot$  in the secular models. The mean merger track SFHs are shown as the thick solid black line, while single merger SFHs are thin grey lines. The dashed line represents the secular SFH for the same formation time  $t_f$ , while the dashed-dotted line represents the secular SFH with the same final mass as the mean merger SFH mass.

epoch of the Universe with some unknown timescale for the duration of the mergers. Indeed, examination of mergers in the Millennium Simulation (Springel et al. 2005) has suggested that mergers do not contribute the majority of stellar mass growth in galaxies, and therefore secular evolution must be the dominant effect (Genel et al. 2008). Newer simulations which also account for detailed baryon physics (Vogelsberger et al. 2014; Genel et al. 2014) will likely shed further light on the importance of mergers for galaxy mass assembly at all redshifts.

For the purposes of our SN Ia age analysis, we need to investigate what effect mergers could have on the distribution of stellar ages across the galaxy mass sequence. To test this, we repeat our galaxy mass assembly process for select tracks and introduce mergers to the process. Specifically, at each time step we calculate a random likelihood of a merger occurring with a total rate of  $0.3 \text{ Gyr}^{-1}$ . We then add the SFH of the building “parent” galaxy to its merging “child” galaxy, assuming the child has undergone secular evolution up to the point of merger. The mass of the child galaxy being merged is chosen from an exponential distribution with mean value 0.2 times the mass of the parent galaxy. After the merger the merged galaxy continues to undergo secular evolution following the SMz relation and quenching prescription as outlined in Section 2 (with additional mergers allowed).

In Figure 11 we show the merged SFHs for four of the selected mass assembly tracks, whose secular tracks correspond to integer intervals in log stellar mass. For each track, we repeat 100 random merger simulations (a subset of which are shown as thin grey lines in each panel), and calculate the mean SFH and mean final mass of the merged galaxies.

Repeating this process for numerous tracks, we again arrive at a prescription for the mean SFH of galaxies as a func-

tion of their total stellar mass. With this we can calculate the predicted CSFH and SN Ia age versus host mass trend. Our merger tracks show an excess of stars at young ages compared to the CSFH predicted by our fiducial models, which further increases the discrepancy with the observed CSFH. This is because the merger effect causes galaxies to have younger average ages for a given stellar mass when compared to the SFH from secular evolution. This also results in slightly younger SN Ia ages at transitional host galaxy mass scales ( $10^{10} - 10^{11} M_{\odot}$ ), but the SN Ia age transition is qualitatively quite consistent with our base model.

#### 5.4 A Fine-Tuned Mass Assembly Model

As some variations to our mass assembly models showed a more favorable agreement with the observed CSFH, we construct a final set of models which incorporates several of these effects. This “fine-tuned” model employs the refit quenching versus redshift relation, the decreased (plateau) high-redshift SMz parametrization, and an additional alteration to the quenching prescription which we now describe.

High-redshift galaxy stellar mass functions have revealed that actively star-forming galaxies may be a non-vanishing component of galaxy populations at *all* galaxy mass scales. Furthermore, many galaxies which evolve off the star-forming main sequence exhibit some residual SF activity (Schawinski 2009), especially those galaxies which quench SF by slowly exhausting their gas reservoir (Schawinski et al. 2014).

To capture this behavior, we enforce a redshift-dependent minimum active galaxy fraction, which manifests as a minimum allowable value for the quenching penalty function (see Appendix A for details). As an example, this minimum SF galaxy fraction at  $z = 2$  is 35%, meaning even the most massive galaxies will retain a SFR of 35% their SMz value. This results in more massive galaxies building their stellar mass over a more extended period of time, resulting in a favorable agreement of the CSFH prediction compared to observations (see Figure 10). Because this “minimum SF fraction” effect is manually constructed to account for a poorly constrained observational effect, we denote this set of models as the “fine-tuned” models.

#### 5.5 SFH Variations: Summary of Results

We explored various alterations to the nominal galaxy mass assembly prescriptions, which show improved agreement with the observed CSFH in some cases and worse agreement in others. Regardless of the galaxy mass assembly details, the transition of SN Ia ages from young SNe in low-mass galaxies to old SNe in high-mass galaxies is preserved in all variations of our models. This is because it is impossible to avert the partitioning of old stars to massive galaxies and young stars to low-mass galaxies. This well-known “downsizing” (Cowie et al. 1996; Faber et al. 2007) of galaxy stellar mass and star-formation is driven by the relationships between sSFR and quiescent galaxy fraction with stellar mass. Consequently, SN Ia ages are affected by the mass assembly history of their host galaxies, and the SN Ia age transition with host mass is unavoidable.

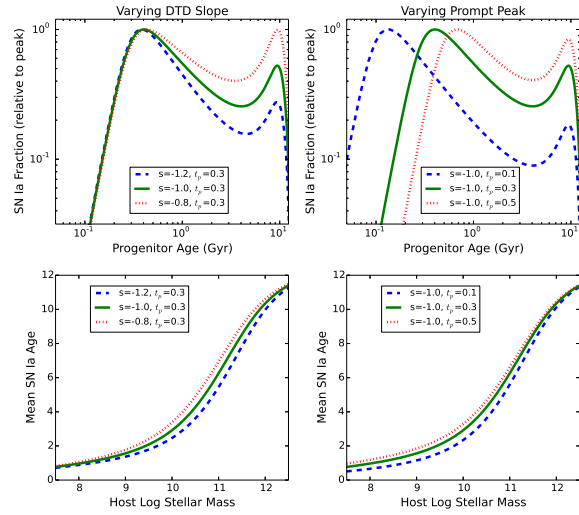


**Figure 12.** Changes in the SN Ia progenitor age distribution at  $z = 0.0$  (top panels) and SN Ia age versus host mass trend (bottom panels) resulting from changes in the SN Ia DTD. Left panels: varying the power law slope  $s$  from Equation 3. Right panels: varying the prompt timescale  $t_p$  of the SN Ia DTD from Equation 3.

### 6 SN Ia AGES: SENSITIVITY TO THE SN Ia DTD

In this Section we inspect how the SN Ia age distribution changes for different forms of the SN Ia DTD. For simplicity and visual clarity, we will focus on how changes in the SN Ia DTD affect the aggregate progenitor age distribution of SNe Ia in the local ( $z = 0.0$ ) Universe.

We begin with altering the general shape of the SN Ia DTD by varying the parameters in Eq. 3. In Figure 12, we show the results of varying the power law slope  $s$  of the DTD (top panel) and the prompt timescale  $t_p$  (bottom panel). Varying the power law slope of the DTD has no effect on the peak age of the prompt component, but has a significant effect on the relative ratio of the prompt and tardy components of the SN Ia progenitor age distribution. Varying the prompt timescale changes not only the peak age of the prompt component (by construction), but also the ratio of prompt to tardy SNe Ia due to the increased relative rate when the prompt component is relatively younger.

While the simple DTD used throughout this work is intentionally artificial, many binary population synthesis studies have been conducted to produce physically realistic DTDs for given progenitor evolution scenarios. We calculate the SN Ia age distributions at  $z = 0$  for select DTDs from the literature coupled to the B13 CSFH. In Figure 13 we show the result for the DD scenario of Mennekens et al. (2010) with  $\alpha = 1.0$  and  $\beta = 1.0$ , the combined SD DTD for WD+RG and WD+MS systems from Hachisu et al. (2008), the  $\gamma - \alpha$  DD model of Toonen et al. (2012), and a select wide DD DTD from Greggio (2005), the DTD from Ruiter et al. (2013) for violent mergers (Pakmor et al. 2012) in the DD scenario (similar to that of Ruiter et al. 2011, but with updated cuts), and the double-detonation (SD) DTD from Ruiter et al. (2014).

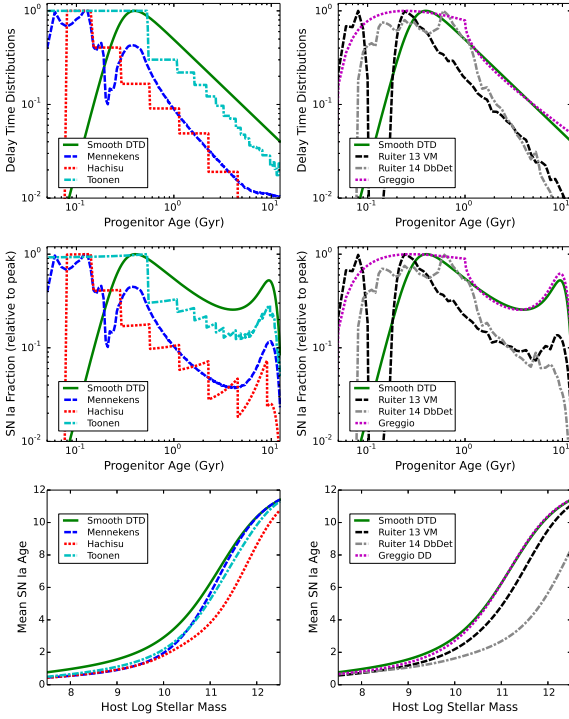


**Figure 13.** Changes in the SN Ia progenitor age distribution at  $z = 0.0$  (middle panels) and SN Ia age versus host mass trend (bottom panels) resulting from the use of various literature DTDs (top panels).

Each of these studies predict multiple DTD outcomes achieved by varying physical assumptions about the physics of binary evolution, and thus produce subtle differences in the final shape of the SN Ia DTD (for a thorough discussion of this topic, see the PopCORN project analysis in Toonen et al. 2014). The qualitative behavior of the final SN Ia age distribution follows the trends identified in Section 3.1. In the young progenitor regime, the SN Ia age distribution follows the shape of the DTD. In the old progenitor regime, the age distribution shows a characteristic bump (the tardy component) of SNe Ia whose progenitor stars formed at the epoch of peak cosmic star formation. A transition of SN Ia ages with host mass is produced for all literature DTDs, even for the most unique DTD (the double-detonation scenario, which is not believed to comprise the *entire* population of SNe Ia). Thus we find the qualitative nature of our results are quite robust against any changes to the specific form of the SN Ia DTD.

## 7 CONCLUSIONS

Using observationally-informed empirical models for galaxy mass assembly, we glean new insight into the origin of the apparent bimodality of SN Ia ages. The “prompt” and “tardy” two-component (or “A+B”) model arises from the bimodal age distribution of SNe Ia realized in nature as a consequence of galaxy star formation histories. We show that this bimodality persists to intermediate redshift ( $z \sim 0.5$ )

and make predictions about the evolution of the two components.

Prompt (young) SNe Ia arise from actively star-forming galaxies, whose star formation histories have evolved slowly compared to the sharp  $t^{-1}$  SN Ia delay time distribution. This results in star-forming galaxies producing SNe Ia predominantly from progenitors whose ages correspond to the peak of the SN Ia DTD, which holds true for all star-forming galaxies at all epochs of cosmic history. Thus prompt SNe Ia originate from similar progenitor ages in all star-forming galaxies at all redshifts, making them the most uniform subset of SNe Ia in the Universe.

Tardy (old) SNe Ia occur in galaxies whose star formation ceased in the distant past. It is only in environments lacking young stars where the SN Ia DTD does not dominate the shape of the SN Ia age distribution. Instead, the SN Ia ages correspond to the past epoch where all the galaxy’s stars were formed. This past epoch of star formation is strongly dependent on the redshift being probed, meaning tardy SNe Ia originate from different progenitor age groups at different redshifts.

These two galaxy SFH regimes which produce the prompt and tardy SNe Ia correspond to different galaxy mass scales. Typically, low-mass galaxies are actively star-forming and thus produce prompt SNe Ia, while massive galaxies have ceased star formation and thus produce tardy SNe Ia. The mean age of SNe Ia undergoes a sharp transition with host mass, similar to that observed in SN Ia Hubble residuals. If the observed Hubble residual step is indeed driven by progenitor age differences, then its magnitude should evolve in redshift in a manner which is not currently accounted for in SN Ia cosmology analyses.

These key results are qualitatively robust, and exhibit negligible sensitivity to the quantitative details of galaxy mass assembly or the SN Ia DTD. Future quantitative refinements will surely be possible with a better measurement of high redshift galaxy populations, particularly the fraction of passive galaxies as a function of stellar mass at very high redshifts. A precise measurement of the SN Ia delay time distribution would then enable quantitative predictions for the potential biases introduced in SN Ia cosmology analyses by the evolution of the progenitor age distribution.

*Acknowledgments:* We are very grateful to Richard Scalzo, Ashley Ruiters, Brian Schmidt, Fuyan Bian, Lee Spitler, Edward (Ned) Taylor, and Aaron Robotham for fruitful discussions. We thank Ashley Ruiters, Nikki Mennekens, Silvia Toonen, and Izumi Hachisu for providing digital representations of their SN Ia DTDs, Jonas Johansson for providing his SN Ia age-stretch relation, and Mark Sullivan and Yen-Chen Pan for providing the PTF host galaxy mass sample. We also thank the anonymous referee for thoughtful feedback on the text, and some very insightful suggestions which particularly strengthened the connection between our models and observations. This research was conducted by the Australian Research Council Centre of Excellence for All-sky Astrophysics (CAASTRO), through project number CE110001020. This research has made use of NASA’s Astrophysics Data System (ADS).

## REFERENCES

- Aubourg, É., Tojeiro, R., Jimenez, R., Heavens, A., Strauss, M. A., & Spergel, D. N. 2008, *A&A*, 492, 631
- Baldry, I. K., Glazebrook, K., Brinkmann, J., Ivezić, Ž., Lupton, R. H., Nichol, R. C., & Szalay, A. S. 2004, *ApJ*, 600, 681
- Baldry, I. K., et al. 2012, *MNRAS*, 421, 621
- Behroozi, P. S., Wechsler, R. H., & Conroy, C. 2013, *ApJ*, 770, 57
- Bell, E. F., McIntosh, D. H., Katz, N., & Weinberg, M. D. 2003, *ApJL*, 585, L117
- Bell, E. F., Phleps, S., Somerville, R. S., Wolf, C., Borch, A., & Meisenheimer, K. 2006, *ApJ*, 652, 270
- Betoule, M., et al. 2013, *A&A*, 552, A124
- . 2014, *arXiv:1401.4064*
- Borch, A., et al. 2006, *A&A*, 453, 869
- Brammer, G. B., et al. 2011, *ApJ*, 739, 24
- Bundy, K., et al. 2006, *ApJ*, 651, 120
- Chabrier, G. 2003, *PASP*, 115, 763
- Childress, M., et al. 2013, *ApJ*, 770, 108
- Conselice, C. J., Rajgor, S., & Myers, R. 2008, *MNRAS*, 386, 909
- Cowie, L. L., Songaila, A., Hu, E. M., & Cohen, J. G. 1996, *AJ*, 112, 839
- D’Andrea, C. B., et al. 2011, *ApJ*, 743, 172
- de Ravel, L., et al. 2009, *A&A*, 498, 379
- Elbaz, D., et al. 2007, *A&A*, 468, 33
- Faber, S. M., et al. 2007, *ApJ*, 665, 265
- Förster, F., Wolf, C., Podsiadlowski, P., & Han, Z. 2006, *MNRAS*, 368, 1893
- Galbany, L., et al. 2012, *ApJ*, 755, 125
- Garn, T., & Best, P. N. 2010, *MNRAS*, 409, 421
- Genel, S., et al. 2008, *ApJ*, 688, 789
- . 2014, *ArXiv e-prints*
- Graur, O., & Maoz, D. 2013, *MNRAS*, 430, 1746
- Graur, O., et al. 2011, *MNRAS*, 417, 916
- . 2014, *ApJ*, 783, 28
- Greggio, L. 2005, *A&A*, 441, 1055
- Gupta, R. R., et al. 2011, *ApJ*, 740, 92
- Hachisu, I., Kato, M., & Nomoto, K. 2008, *ApJL*, 683, L127
- Hayden, B. T., Gupta, R. R., Garnavich, P. M., Mannucci, F., Nichol, R. C., & Sako, M. 2013, *ApJ*, 764, 191
- Howell, D. A., Sullivan, M., Conley, A., & Carlberg, R. 2007, *ApJL*, 667, L37
- Howell, D. A., et al. 2009, *ApJ*, 691, 661
- Hoyle, F., & Fowler, W. A. 1960, *ApJ*, 132, 565
- Iben, Jr., I., & Tutukov, A. V. 1984, *ApJS*, 54, 335
- Johansson, J., et al. 2013, *MNRAS*, 435, 1680
- Karim, A., et al. 2011, *ApJ*, 730, 61
- Kashino, D., et al. 2013, *ApJL*, 777, L8
- Kelly, P. L., Hicken, M., Burke, D. L., Mandel, K. S., & Kirshner, R. P. 2010, *ApJ*, 715, 743
- Kim, A. G., et al. 2013, *ApJ*, 766, 84
- . 2014, *ApJ*, 784, 51
- Konishi, K., et al. 2011, *ArXiv e-prints*
- Lampeitl, H., et al. 2010, *ApJ*, 722, 566
- Lee, J. C., et al. 2009, *ApJ*, 706, 599
- Leitner, S. N. 2012, *ApJ*, 745, 149
- Leitner, S. N., & Kravtsov, A. V. 2011, *ApJ*, 734, 48
- Li, W., Chornock, R., Leaman, J., Filippenko, A. V., Poznanski, D., Wang, X., Ganeshalingam, M., & Mannucci, F. 2011, *MNRAS*, 412, 1473
- Madau, P., & Dickinson, M. 2014, *ArXiv e-prints*
- Mannucci, F., Della Valle, M., & Panagia, N. 2006, *MNRAS*, 370, 773
- Mannucci, F., Della Valle, M., Panagia, N., Cappellaro, E., Cresci, G., Maiolino, R., Petrosian, A., & Turatto, M. 2005, *A&A*, 433, 807
- Maoz, D., & Mannucci, F. 2012, *PASA*, 29, 447
- Maoz, D., Mannucci, F., Li, W., Filippenko, A. V., Valle, M. D., & Panagia, N. 2011, *MNRAS*, 412, 1508
- Mennekens, N., Vanbeveren, D., De Greve, J. P., & De Donder, E. 2010, *A&A*, 515, A89+
- Mosher, J., et al. 2014, *arXiv:1401.4065*
- Moustakas, J., et al. 2013, *ApJ*, 767, 50
- Muzzin, A., et al. 2013, *ApJ*, 777, 18
- Neill, J. D., et al. 2009, *ApJ*, 707, 1449
- Noeske, K. G., et al. 2007, *ApJL*, 660, L43
- Nomoto, K. 1982, *ApJ*, 253, 798
- Pakmor, R., Kromer, M., Taubenberger, S., Sim, S. A., Röpke, F. K., & Hillebrandt, W. 2012, *ApJL*, 747, L10
- Pan, Y.-C., et al. 2014, *MNRAS*, 438, 1391
- Pannella, M., et al. 2009, *ApJL*, 698, L116
- Perlmutter, S., et al. 1999, *ApJ*, 517, 565
- Perrett, K., et al. 2012, *AJ*, 144, 59
- Rest, A., et al. 2013, *arXiv:1310.3828*
- Riess, A. G., et al. 1998, *AJ*, 116, 1009
- Rigault, M., et al. 2013, *A&A*, 560, A66
- Robotham, A. S. G., et al. 2014, *ArXiv e-prints*
- Rodney, S. A., et al. 2014, *AJ*, 148, 13
- Ruiter, A. J., Belczynski, K., Sim, S. A., Hillebrandt, W., Fryer, C. L., Fink, M., & Kromer, M. 2011, *MNRAS*, 417, 408
- Ruiter, A. J., Belczynski, K., Sim, S. A., Seitenzahl, I. R., & Kwiatkowski, D. 2014, *MNRAS*, 440, L101
- Ruiter, A. J., et al. 2013, *MNRAS*, 429, 1425
- Salim, S., et al. 2007, *ApJS*, 173, 267
- Scannapieco, E., & Bildsten, L. 2005, *ApJL*, 629, L85
- Schawinski, K. 2009, *MNRAS*, 397, 717
- Schawinski, K., et al. 2014, *MNRAS*, 440, 889
- Scolnic, D., et al. 2013, *arXiv:1310.3824*
- Scolnic, D. M., Riess, A. G., Foley, R. J., Rest, A., Rodney, S. A., Brout, D. J., & Jones, D. O. 2014, *ApJ*, 780, 37
- Smith, M., et al. 2012, *ApJ*, 755, 61
- Spitler, L. R., et al. 2014, *ApJL*, 787, L36
- Springel, V., et al. 2005, *Nature*, 435, 629
- Stark, D. P., Schenker, M. A., Ellis, R., Robertson, B., McLure, R., & Dunlop, J. 2013, *ApJ*, 763, 129
- Stratman, C. M. S., et al. 2014, *ApJL*, 783, L14
- Sullivan, M., et al. 2006, *ApJ*, 648, 868
- . 2010, *MNRAS*, 406, 782
- . 2011, *ApJ*, 737, 102
- Suzuki, N., et al. 2012, *ApJ*, 746, 85
- Taylor, E. N., et al. 2014, *ArXiv e-prints*
- Tomczak, A. R., et al. 2014, *ApJ*, 783, 85
- Toonen, S., Claeys, J. S. W., Mennekens, N., & Ruiter, A. J. 2014, *A&A*, 562, A14
- Toonen, S., Nelemans, G., & Portegies Zwart, S. 2012, *A&A*, 546, A70
- Totani, T., Morokuma, T., Oda, T., Doi, M., & Yasuda, N. 2008, *PASJ*, 60, 1327
- Tutukov, A. V., & Iungelson, L. R. 1976, *Astrofizika*, 12, 521



- Tutukov, A. V., & Yungelson, L. R. 1979, *AcA*, 29, 665  
 Vogelsberger, M., et al. 2014, arXiv:1405.2921  
 Webbink, R. F. 1984, *ApJ*, 277, 355  
 Whelan, J., & Iben, Jr., I. 1973, *ApJ*, 186, 1007  
 Whitaker, K. E., van Dokkum, P. G., Brammer, G., & Franx, M. 2012, *ApJL*, 754, L29  
 Wolf, C., Gray, M. E., & Meisenheimer, K. 2005, *A&A*, 443, 435  
 Wolf, C., et al. 2009, *MNRAS*, 393, 1302  
 Yungelson, L. R., & Livio, M. 2000, *ApJ*, 528, 108  
 Zahid, H. J., Dima, G. I., Kewley, L. J., Erb, D. K., & Davé, R. 2012, *ApJ*, 757, 54  
 Zahid, H. J., Yates, R. M., Kewley, L. J., & Kudritzki, R. P. 2013a, *ApJ*, 763, 92  
 Zahid, H. J., et al. 2013b, ArXiv e-prints

## APPENDIX A: GALAXY MASS ASSEMBLY: PARAMETRIZATION OF MODELS

This Appendix presents the formal parametrizations for all input scaling relations employed in our galaxy mass assembly models.

### A1 Nominal SFH Parametrizations

The nominal relationship between stellar mass and star formation rate as a function of redshift (the SMz relation) is formally defined in Z12 as:

$$\Psi(M_*, z) = 2.00 \cdot \exp(1.33z) \left( \frac{M_*}{10^{10}} \right)^{0.7} [M_\odot \text{yr}^{-1}] \quad (\text{A1})$$

Stellar mass loss as a function of time after epoch of star formation is given by LK11 for a variety of IMFs. For our Chabrier (2003) IMF this parametrization is:

$$f_{ml}(t) = 0.046 \ln \left( \frac{t}{0.276 \text{ Myr}} + 1 \right) \quad (\text{A2})$$

To accurately account for the redshift evolution of the quenching mass, we use the parametrization of Muzzin et al. (2013), which is anchored at  $\log(M_*/M_\odot) = 10.55$  at  $z = 0.35$ . Explicitly, our parametrization for the quenching mass as a function of redshift is:

$$\log \left( \frac{M_Q(z)}{M_\odot} \right) = \begin{cases} 10.43 + 0.9 \log(1+z) & : z \leq 1.5 \\ 8.56 + 5.6 \log(1+z) & : z > 1.5 \end{cases} \quad (\text{A3})$$

To account for the gradual transition from active galaxies at low stellar mass to passive galaxies at high stellar mass, we impose a quenching penalty function of the form:

$$p_Q(M_*, z) = \frac{1}{2} \left[ 1 - \text{erf} \left( \frac{\log(M_*) - \log(M_Q(z))}{\sigma_Q} \right) \right] \quad (\text{A4})$$

where  $M_Q(z)$  is the quenching mass as a function of redshift. Our nominal value for the quenching mass transition scale is  $\sigma_Q = 1.5$ , which is a good representation of the active galaxy fraction for the galaxy stellar mass functions calculated in the low redshift universe by Moustakas et al. (2013). In Figure A1 we show these mass functions and the nominal  $\sigma_Q = 1.5$  quenching penalty function (right panels), as well as the “narrow quenching” width ( $\sigma_Q = 1.1$ ) penalty function which is a good fit to the GAMA (Baldry et al. 2012) mass functions (left panels).

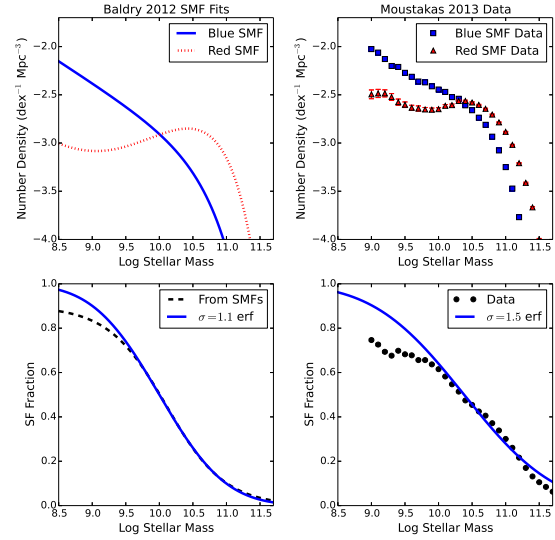


**Figure A1.** Top left: blue and red galaxy stellar mass functions (SMFs) from GAMA (Baldry et al. 2012). Bottom left: blue (i.e., SF) galaxy fraction as a function of mass for GAMA (dashed black curve) and *erf* model with width  $\sigma_Q = 1.1$ . Top right: blue and red galaxy number densities as a function of mass for SDSS+*GALEX* from Moustakas et al. (2013). Bottom right: blue (SF) galaxy fraction versus mass from data (black points) and *erf* model with width  $\sigma_Q = 1.5$ .

Finally, with all these parametrizations in hand (Equations A1, A2, A3, A4), we have the components necessary to explicitly integrate the galaxy stellar mass assembly using the following equation:

$$\frac{M_*(t + \Delta t) - M_*(t)}{\Delta t} = p_Q(M_*(t), z(t)) \cdot \Psi(M_*(t), z(t)) - \frac{\Delta M_*}{\Delta t} \quad (\text{A5})$$

where the mass lost in each time interval is a sum of mass lost from stars formed in each previous time step:

$$\Delta M_* = \int_0^{t-t_f} \Psi(M_*(t-\tau), z(t-\tau)) \cdot (f_{ml}(\tau + \Delta t) - f_{ml}(\tau)) d\tau \quad (\text{A6})$$

### A2 Alternate SFH Parametrizations

The alternate parametrizations for galaxy mass assembly model inputs are displayed graphically in Figure A2, and are described in turn below.

Our alternate parametrization for the SMz relation is:

$$\Psi(M_*, z) = 36.4 \cdot \left( \frac{M_*}{10^{10}} \right)^{0.7} \cdot \frac{\exp(1.9z)}{\exp(1.7z) + \exp(0.2z)} \quad (\text{A7})$$

This is a hand-constructed formula which has the same mass dependence as the Z12 relation but a different redshift dependence. It matches the Z12 SMz relation well below  $z = 2$  but becomes much shallower above  $z = 2$ . In the top left panel of Figure A2, we show the SFR for a  $M_* = 10^{10} M_\odot$  galaxy as a function of redshift for both parametrizations.

Next we fit for a different functional form of the quenching mass as a function of redshift  $M_Q(z)$  using several data



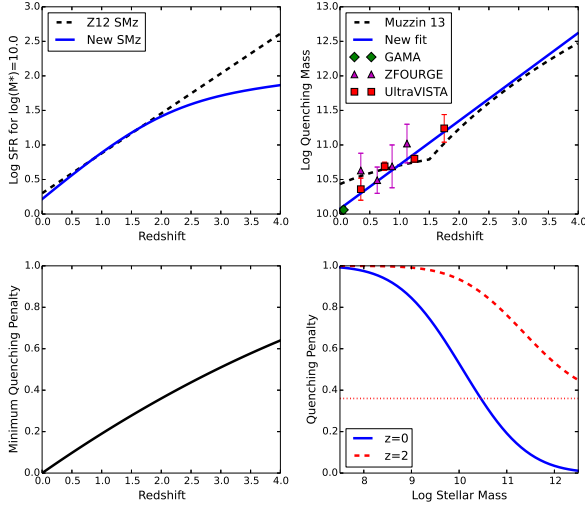


**Figure A2.** Top left: SFR for a  $\log(M_*/M_\odot) = 10$  galaxy as a function of redshift for the Z12 SMz relation (dashed black line, Eq. A1) and the modified SMz (solid blue line, Eq. A7). Top right: Quenching mass data (points), original quenching versus redshift formula (dashed black line, Eq. A3) from Muzzin et al. (2013), and new linear fit to the data (solid blue line, Eq. A8). Bottom left: Minimum quenching penalty versus redshift in for the “fine-tuned” model. Bottom right: quenching penalty versus mass at two redshifts (solid blue curve  $z = 0$ , dashed red curve  $z = 2$ ) for the “fine-tuned” model (Eq. A9).

sets. To do so, we use data sets where the blue and red stellar mass functions are well-fit and show a clear quenching mass scale where the quiescent fraction crosses 50%. The final data sets we employ are the  $z = 0.06$  GAMA point (Baldry et al. 2012), the three lowest redshift bins from UltraVISTA (Muzzin et al. 2013), and the four lowest redshift points from ZFOURGE (Tomczak et al. 2014). These data points are extremely well fit by a linear function of the form:

$$\log(M_Q(z)/M_\odot) = 10.077 + 0.636 \cdot z \quad (\text{A8})$$

The top right panel of Figure A2 shows the data points employed in our fit, the new fit  $M_Q(z)$ , and the original Muzzin et al. (2013) parametrization.

Finally, for our “fine-tuned” model we employed a minimum quenching penalty value which evolves quadratically from 0% at redshift  $z = 0$  to 100% at redshift  $z = 10$ . Formally this manifests in the quenching penalty equations as:

$$\begin{aligned} \bar{p}_Q(M_*, z) &= p_{\min}(z) + (1 - p_{\min}(z)) \cdot p_Q(M_*, z) \\ p_{\min}(z) &= 1 - \left( \frac{z - 10}{10} \right)^2 \end{aligned} \quad (\text{A9})$$

The bottom left panel of Figure A2 shows the minimum quenching penalty as a function of redshift, while the bottom right panel shows an example of the quenching penalty functions at  $z = 0$  and  $z = 2$  in the new parametrization.